JOURNAL OF ELECTROMAGNETIC ENGINEERING AND SCIENCE, VOL. 24, NO. 3, 254~263, MAY. 2024

https://doi.org/10.26866/jees.2024.3.r.226
ISSN 2671-7263 (Online) · ISSN 2671-7255 (Print)

Mechanism and Method for Residual Flux Detection of Transformer Cores Based on Different Polarities Response Currents

Cailing Huo[1] · Yiming Yang[1,*] · Fuyin Ni[1] · Qiang Xie[2]

Abstract

This paper proposes a residual flux detection method based on the different polarities of response currents. When a positive–negative alternating DC voltage is loaded, the direction of the residual flux can be determined by the difference between the various polarities of the response current waveforms. As a result, residual flux value can be calculated using the empirical formula that relates residual flux to the responce current. In this formula, unknown parameters can be obtained using the field-circuit coupling method. Finally, this paper employs a closed iron core as an example to obtain the corresponding formula and then verifies its accuracy through experiments. The results show that the accuracy of the proposed method is less than 5%, which is higher than that of other existing methods. The method presented in this paper not only accurately detects the residual flux of a transformer but also requires no additional energy from the transformer.

Key Words: Different Polarity Response Currents, Empirical Formula, Power Transformer, Residual Flux.

I. Introduction

A power transformer is one of the most significant and expensive equipment employed in a power grid. As a result, safe operation of the power transformer is crucial for a power system [1]. Transformer core materials generally feature hysteresis and saturation characteristics [2], due to which an unknown residual flux (RF) may be generated in their iron core after a DC resistance test, a transformation ratio measurement, or a no-load closing operation [3]. If this RF is large, a large amount of inrush current may form when the transformer is turned off, which can lead to winding deformation, current imbalance, and harmonic pollution [4]. Such situations render the transformer protection function invalid. Therefore, research on RF detection mechanisms and methods has important academic significance for reducing inrush current [5].

At present, an empirical method is often used to estimate magnetic flux, according to which the RF is estimated based on the 0.2–0.7 saturation flux [6–8]. However, this estimation error depends on historical experience, which is not conducive to on-site detection. The second method is the induced voltage method, which is based on the electromagnetic induction law for detecting magnetic flux changes in the magnetic core [9]. It calculates the RF by recording the induced voltage waveform when the transformer is turned off. However, since the RF calculated on starting the transformer is always different from the stabilized RF [10],

Manuscript received May 31, 2023 ; Revised October 07, 2023 ; Accepted December 08, 2023. (ID No. 20230531-099J)
[1]School of Electrical and Information Engineering, Jiangsu University of Technology, Changzhou, China.
[2]Changzhou Power Supply Branch of State Grid Jiangsu Electric Power Co. Ltd., Changzhou, China.
[*]Corresponding Author: Yiming Yang (e-mail: yym2022@jsut.edu.cn)

the feasibility of this method is limited in practical application. The third method is the pre-magnetization method [11], which involves pre-charging the iron core with a known RF to then use phase-selective closing technology or the demagnetization method to suppress the inrush current. However, this method cannot pre-charge a certain amount of RF in advance for the actual transformer core, which limits its feasibility in practice.

The RF formation process involves complex changes in the magnetic domain structure of ferromagnetic materials [12]. Therefore, some previous studies have also studied indirect detection methods. In [13], RF was measured by analyzing the magnetic leakage around the iron core. Although this method was able to detect RF, it was limited by the influence of different measuring points on the measurement results, ultimately achieving a measurement accuracy as high as 20%. In [14], RF was estimated by analyzing the magnetized inductance. However, its measurement results were limited by the accuracy of the iron core model In addition, an RF detection method based on even the harmonics of the induced voltage is presented in [15], which was able to detect the RF of the current transformer, but its accuracy was limited by the accuracy of the simulation model. In [16], an RF detection method using small loop energy is proposed, but this method ignores the energy change under small RF, thus increasing the error of the extraction relationship. In [17], an RF detection method based on phase difference was analyzed, but the phase difference obtained by this method under different RFs was small, which is not conducive to its detection in practice. Furthermore, [18–20] studied RF detection methods considering transient variables, but the test time of the measured waveform was difficult to extract, rendering the accuracy of the detection results unstable and not conducive to on-site testing. Based on the above research methods, it is evident that there is still no fast and effective RF detection method available.

This paper presents an RF detection method based on the different polarities of response currents to obtain an accurate RF value and polarity. First, when the DC voltage in different directions is loaded in sequenc, the RF detection mechanism is analyzed, and a method for determining the RF direction is proposed. Following this, the relationship between the RF and the response current is established, and the corresponding parameters are obtained by employing the field-circuit coupling method. Finally, an RF test platform for a square core is built to verify the feasibility of the theoretical analysis and the accuracy of the proposed method.

II. Detection Principle of Residual Flux

The RF formation mechanism based on different magnetized states is depicted in Fig. 1, indicating that when the magnetic field strength H gradually increases to reach its maximum value, the magnetic flux increases along $0ab$. Furthermore, when the external magnetic field disappears at point a or b due to hysteresis characteristics, a different RF is generated in the iron core, such as B_r or B_r'. Therefore, it is evident that RF generation is primarily decided by changes in the domain structure at the RF, which can be reflected by changes in the relative differential permeability (μ_{rd}), expressed as follows:

$$\mu_{rd} = \frac{1}{\mu_0}\frac{\Delta B}{\Delta H} \tag{1}$$

where μ_0 is a constant, referring to the vacuum permeability of air, and ΔB and ΔH are the increments of B and H, respectively.

To analyze the variation trend of differential permeability at RF, this paper analyzed the material characteristics of the iron core using the silicon-steel sheets (model B30P105). The hysteresis loop of the core at low frequencies was measured, after which the differential permeability trend caused by saturation to the RF state was analyzed, as shown in Fig. 2. It is observed that when the frequency is 5 Hz, the B_m reaches 1.8 T, while the coercive force H_c is 13 A/m, indicating the difficulty involved in magnetizing the material. Furthermore, when ΔH is greater than 5% of H_c, the difference between the positive relative permeability μ_{rp} and negative relative permeability μ_{rn} is quite obvious. At this juncture, the relationship between μ_{rp} and μ_{rn} can be expressed as follows:

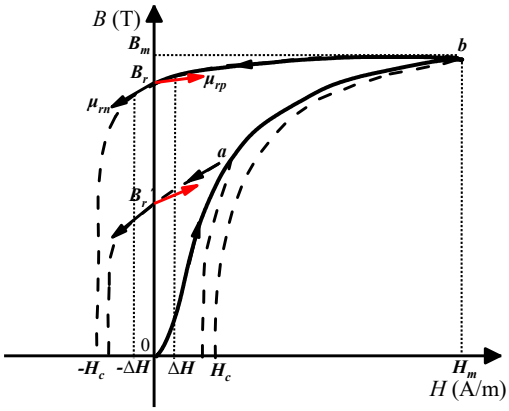

Fig. 1. Formation mechanism of residual flux under different magnetization states.

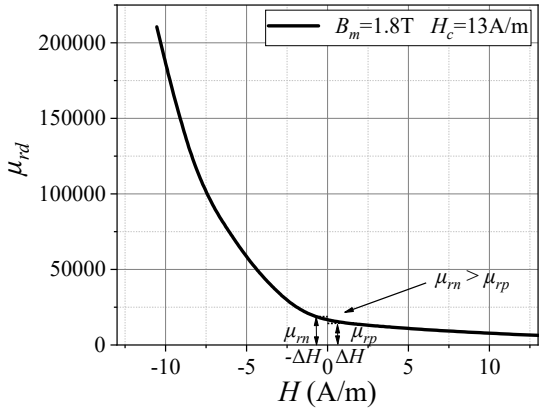

Fig. 2. Variation trend of μ_{rd} caused by saturation to the residual flux state.

$$\mu_{rp} < \mu_{rn}. \tag{2}$$

Based on the above relationship, the RF direction can be judged by comparing μ_{rp} with μ_{rn}. However, measuring μ_{rp} and μ_{rn} is not an easy task, due to the complex changes occurring in the magnetic domain structure. Therefore, it is necessary to analyze an indirect variable that can reflect μ_{rd}. Notably, when a DC voltage is loaded on one side of the winding of a transformer, the quantitative detection of RF can be realized by analyzing the relationship between the response current and the μ_{rd} in the circuit.

After the transformer is turned off, the method proposed in this paper only needs to connect the designed DC measurement circuit to a winding located close to the iron core for response current sensing. Subsequently, by analyzing the relationship between the response current and the RF, quantitative detection of the RF can be realized. Fig. 3 presents the DC detection circuit, where $u_s(t)$ is the DC voltage and R_s denotes the series resistance. In an actual operation, when a transformer is reconnected to the power system, the RF direction remains unknown. To address this issue, the current paper analyzed the relationship between the RF and the response current under different excitation directions of the applied voltage. The main waveforms generated by applying the DC excitation directions are presented in Fig. 4. First, a positive DC voltage with the same polarity as the initial RF density was applied, after which a negative DC voltage was introduced—this waveform is abbreviated as PN. Similarly, a negative DC voltage with a polarity opposite to the initial RF density was applied, after which a positive DC voltage was implemented—this waveform is abbreviated as NP.

As shown in Fig. 4, in the case of PN, when the positive voltage is loaded first at t_1, the positive respond current $i_p(t)$ is generated. When the voltage is removed after t_2, the RF in the iron core becomes a new B_{rp}. Subsequently, when the negative voltage with a polarity opposite to the RF is applied at t_3, a negative respond current $i_n(t)$ is generated. After t_4, when the voltage is removed, the initial RF changes from B_{rp} to B_{rn}. However, in the case of NP, as shown in Fig. 4(b), $i_n(t)$ is produced first and $i_p(t)$ is produced second, due to which the initial RF first changes to B_{rn} and then to B_{rp}. According to Eq. (2), μ_{rp} at RF is less than μ_{rn}, due to which the changes in RF are different in the case of PN and NP. Thus, the waveforms of the measured positive and negative respond current are also different. Consequently, the quantitative detection of the RF was realized by means of this difference.

When a voltage is loaded, the transformer core becomes equivalent to an *RL* series-parallel circuit. Fig. 5 shows an equivalent circuit model for the measurement circuit, where R_s represents the total resistance in the circuit, primarily including the series resistance and winding resistance. Meanwhile, L_{eq} stands for the equivalent magnetized inductance of the iron core, which is related to the change in magnetic flux. R_{Fe} stands for hysteresis loss in transient processes, also called iron loss resistance. Notably, when the turns of the winding (*N*), the cross-sectional area *S*, and the average magnetic circuit length *l* are known, the magnetization inductance L_{eq} at the RF can be related to the differential permeability μ_{rd}.

According to the magnetic circuit analysis, the relationship between L_{eq} and μ_{rd} can be expressed as:

$$L_{eq} = \frac{N^2 S \mu_0}{l} \mu_{rd}. \tag{3}$$

Furthermore, since the applied excitation is DC excitation, the time constant in the measurement circuit can be expressed as L_{eq}/R. Therefore, the respond current $i(t)$ in the circuit can be formulated as follows:

$$i(t) = I_o \left(1 - e^{-\frac{t}{\frac{1}{R}\frac{N^2 S \mu_0}{l}\mu_{rd}}}\right) = I_o \left(1 - e^{-\frac{t}{k\mu_{rd}}}\right), \tag{4}$$

where R represents the parallel connection between R_{Fe} and R_s. Furthermore, according to Eq. (4), $i_p(t)$ and $i_n(t)$ are represented as follows:

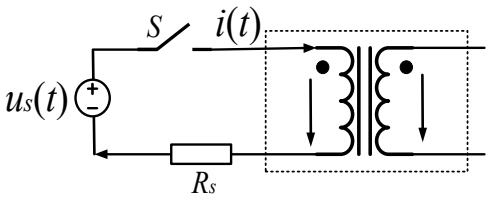

Fig. 3. DC measurement circuit.

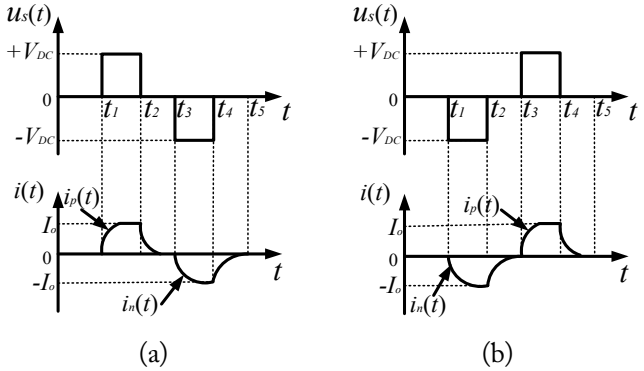

Fig. 4. Main waveforms: (a) PN and (b) NP.

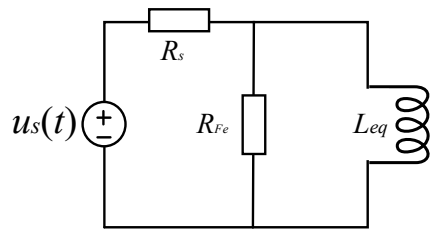

Fig. 5. Equivalent circuit model.

$$\begin{cases} i_p(t) = I_o\left(1 - e^{-\frac{t}{k\mu_{rp}}}\right) \\ i_n(t) = I_o\left(1 - e^{-\frac{t}{k\mu_{rn}}}\right) \end{cases}. \quad (5)$$

Based on Eqs. (2) and (5), the relationship between $i_p(t)$ and $i_n(t)$ can be obtained from the following formula:

$$i_p(t) > i_n(t). \quad (6)$$

Regardless of whether the positive or negative excitation was loaded first, the change rate of $i_p(t)$ was found to be faster than that of $i_n(t)$. Therefore, the RF direction can be judged by comparing the waveforms $i_p(t)$ and $i_n(t)$. Notably, to obtain the relationship between RF and the response current, μ_{rd} can be expressed as follows:

$$\mu_{rd} = -\frac{t_s l R}{N^2 S \mu_0} \frac{1}{\ln\left(1 - \frac{1}{I_o} \cdot i(t_s)\right)}, \quad (7)$$

where t_s is the best measurement time for the respond current. According to Eq. (7), the change in the magnetic domain structure at RF maintains a pertinent relationship with respond current. Therefore, this study proposes a method for calculating the RF by establishing a relationship between B_r and $i(t_s)$. This relationship can be expressed as follows:

$$B_r = f\big(i(t_s)\big) = \frac{a}{\ln\big(1 - 1/I_o \cdot i(t_s)\big)} + b, \quad (8)$$

where a and b are constant coefficients whose values are determined by the finite element method, and I_o represents the current value when the circuit reaches a steady state, which can be expressed as V_{DC}/R.

In the following sections, the field-circuit coupling method is applied to analyze the above relationship, and an experimental verification is carried out.

III. Field-Circuit Coupling Analysis

This paper used the finite element method to extract empirical formulas for calculating RF. First, the iron core was modeled. To simulate the initial RF in the iron core, the hysteresis model of the iron core was used during modeling. In particular, the J-A hysteresis model presented in [21] was employed to simulate the hysteresis characteristics of the iron core and achieve an accurate simulation of its initial RF. The five parameter values of the hysteresis model obtained through parameter identification were M_s = 1.58 × 10^6 A/m, a = 4.56 A/m, *alpha* = 5.67 × 10^{-6}, k = 8.95 A/m, and c = 0.18. Fig. 6 depicts the research objects selected for this study. As shown, S of the iron core is 0.0016 m^2, l of the iron core is 1.92 m, and N of the measuring winding is 50.

Notably, before DC excitation loading, the initial RF needs to be preset in the core. In this study, the initial RF was simulated by applying a short-term large current to the core. First, a large current was applied to the winding so that the magnetic flux of the core quickly reached its maximum value. Subsequently, the large current was removed, with the static flux in the core being the initial RF of the simulation. As shown in Fig. 6, when the initial RF is 0.845 T, the magnetic flux inside the core is larger than that outside the core. This can be attributed to the shorter magnetic circuit length of the inner side and the smaller magnetic resistance of the core, which makes the magnetic flux larger. The error between the internal and external magnetic flux with regard to the average magnetic flux was less than 0.12%, indicating that the distribution of magnetic flux at the RF was almost uniform.

1. Selection of Independent Variables

Fig. 7 traces the waveforms of the preset current, the loaded DC voltage, the flux density, and the respond current for PN and NP. It is evident that when $i_p(t)$ reaches the steady state (the current value is 0.043 A), $i_n(t)$ has not yet reached the steady state (the current value is 0.029 A). As a result, the value of $i_p(t)$ is greater than that of $i_n(t)$—consistent with the theoretical analysis. Furthermore, Fig. 7 shows that when a positive voltage is applied, the RF change remains within 0.001 T, thus remaining almost unchanged. However, when a negative voltage is applied, the RF change is large than that caused by the positive voltage. This indicates that while $i_n(t)$ is generated at almost the same B_r (0.845 T and 0.846 T), $i_p(t)$ is generated at a different B_r (0.845 T and 0.808 T). Therefore, if $i_p(t)$ is selected to measure the RF in the iron core, a large error may occur in the measurement. However, if $i_n(t)$ is selected, the error would be greatly reduced. Therefore, to improve measurement accuracy, this paper considered $i_n(t)$ as the independent variable for detecting the RF in the iron core.

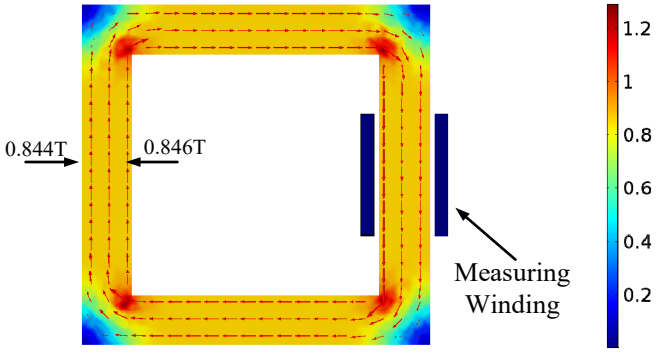

Fig. 6. Square iron core model in finite-element method (FEM).

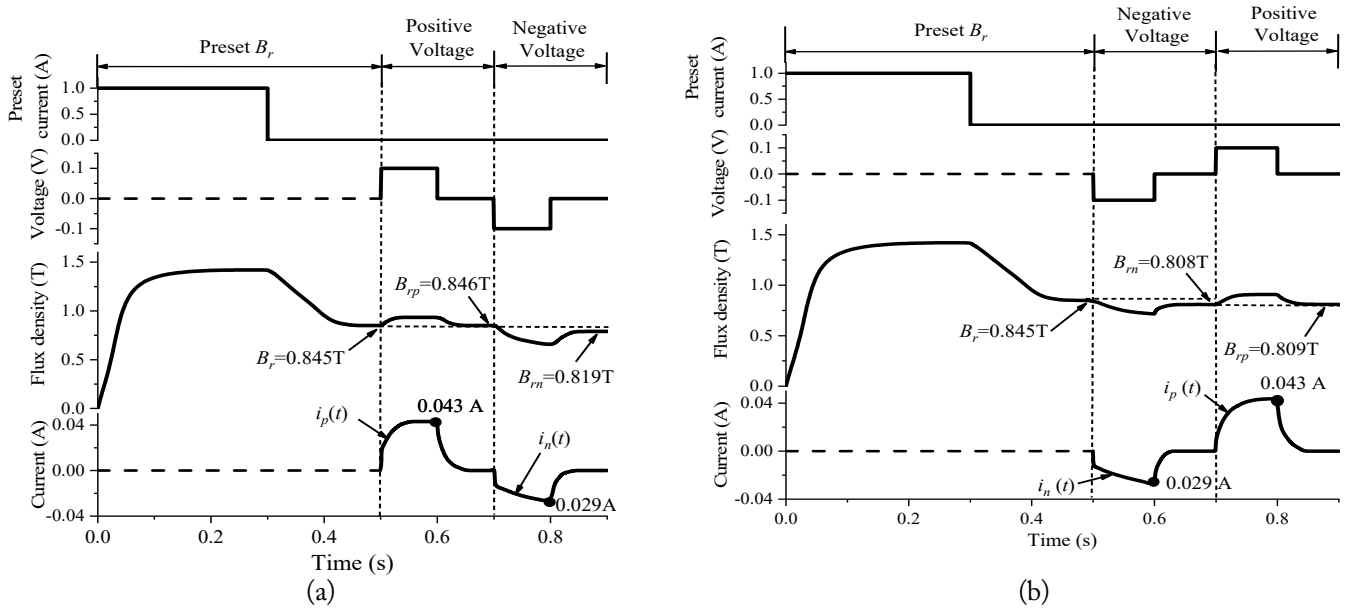

Fig. 7. The main waveforms in the finite-element method (FEM): (a) PN and (b) NP.

2. Selection of Load Voltage

In Fig. 7(a), the initial RF changes from 0.846 T to 0.819 T, with the change rate of negative B_r being 3.19%. Meanwhile, in Fig. 7(b), the initial RF changes from 0.845 T to 0.808 T, with the change rate of negative B_r being 4.38%. This indicates that the influence of negative voltage on RF is relatively obvious in the case of NP. As a result, the maximum range of the applied excitation was obtained by analyzing the RF change rate under NP. Fig. 8 traces the change in trend of negative B_r under NP, where parameter k is the ratio of H_1 $(H_1 = \Delta H)$ to the coercive force H_c, reflecting the influence of the loaded voltage on RF. Notably, when $k > 0.13$, the B_r% exceeds 5%. Therefore, this study considers the change in B_r to be less than 5% when DC voltage is applied. In addition, when H_1 is not greater than 5% of H_c in Fig. 2, the change in μ_{rp} and μ_{rn} may not be very obvious, which may make it impossible to determine the RF direction. Thus, the value of k is selected as 0.05 to 0.13 of the H_c.

Based on the ampere loop law, the following equation can be formulated:

$$I_o \cdot N = H_1 \cdot l. \tag{9}$$

The applied V_{DC} can be expressed as follows:

$$V_{DC} = \frac{H_1 \cdot l \cdot R}{N}. \tag{10}$$

Therefore, when the range of k $(k = H_1/H_c)$ is from 0.05 to 0.13, the range of the applied V_{DC} can be formulated as follows:

$$\frac{0.05H_c \cdot l \cdot R}{N} \le V_{DC} \le \frac{0.13H_c \cdot l \cdot R}{N}. \tag{11}$$

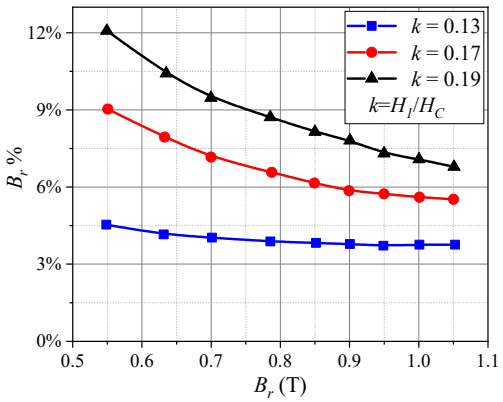

Fig. 8. Change rate of negative B_r at NP.

Furthermore, when the parameters are $N = 50$, $R = 2.32\ \Omega$, and $H_c = 13$ A/m, the range of the applied V_{DC} can be considered as follows:

$$0.058V \le V_{DC} \le 0.151V. \tag{12}$$

3. Determination of Best Measurement Time

According to the determined core material characteristics and external circuit parameters, finite element simulation analysis was carried out to obtain the respongise current under different RFs. Subsequently, the best measurement time for the response current was selected to investigate the relationship between different RFs and the response current.

Fig. 9 shows the waveforms of $i_p(t)$ and $i_n(t)$ at different RFs when the voltage is 0.1 V. It is evident that the current values obtained at different moments are different. This made it necessary to analyze the relationship between the current value at different moments and the RF. As shown in Fig. 10, when the

time is 0.025 seconds, the change in trend of $i_p(t)$ with an increase in RF is different under PN than under NP (Fig. 10(a)). However, when the time is 0.1 seconds, the change trend of $i_n(t)$ is basically the same for the two cases (Fig. 10(b)). This may be attributed to the fact that when positive voltage is applied, the initial RF is different for both cases, whereas when negative voltage is applied, the initial RF remains unchanged. This indicates that, while the generated $i_n(t)$ basically remains the same, $i_p(t)$ is different in the two cases. Therefore, to accurately calculate the RF in different directions, this paper chose $i_n(t)$ as the measurable variable to calculate the RF in the iron core. Furthermore, the best measurement time t_s was selected as 0.1 seconds, indicating the moment when the voltage would be removed. Notably, at this time, the values of $i_n(t)$ calculated from the experiment would be easier to measure and the difference in current values would also be more obvious.

After determining the best measurement time for the response current, the empirical formula for calculating RF was obtained by analyzing the relationship between respond current and RF using the data fitting method. Since the basic functional form of the fitting formula had already been determined by drawing on Eq. (8), only the parameter values had to be determined. Therefore, considering that the time is 0.1 seconds, the voltage is 0.1 V, and the total resistance is 2.32 Ω, the relationship between $i_n(t)$ and B_r can be fitted as follows:

$$B_r = \frac{a}{\ln\left(1 - 23.26 \cdot i_n(t_s)\right)} + b. \tag{13}$$

Here, the values for a and b were obtained by the data fitting method as 0.67 and 1.45, respectively.

IV. Experimental Validation

An RF detection platform comprising a square iron core was

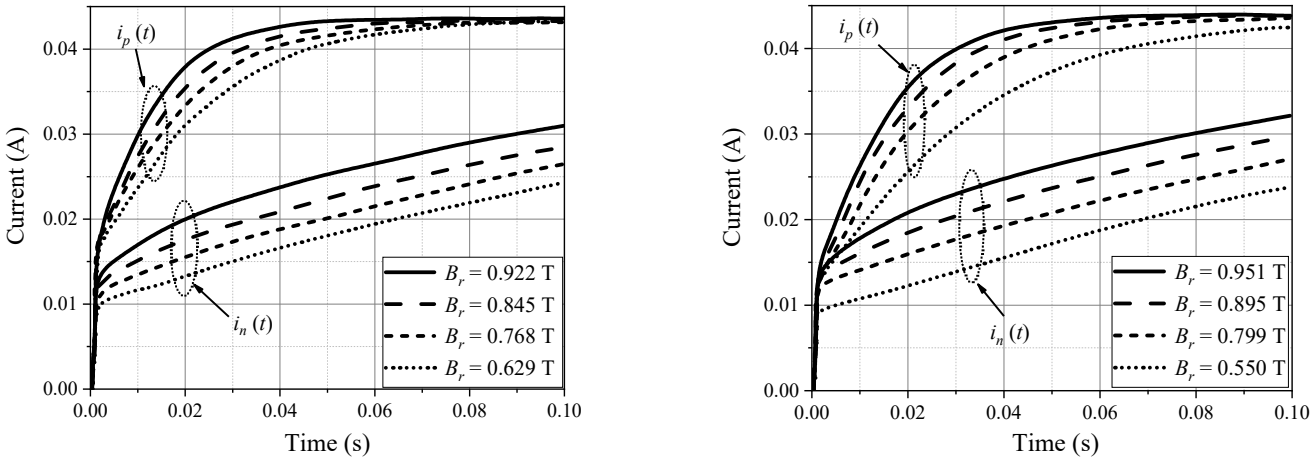

Fig. 9. Waveforms of $i_p(t)$ and $i_n(t)$ at different residual fluxes: (a) PN and (b) NP.

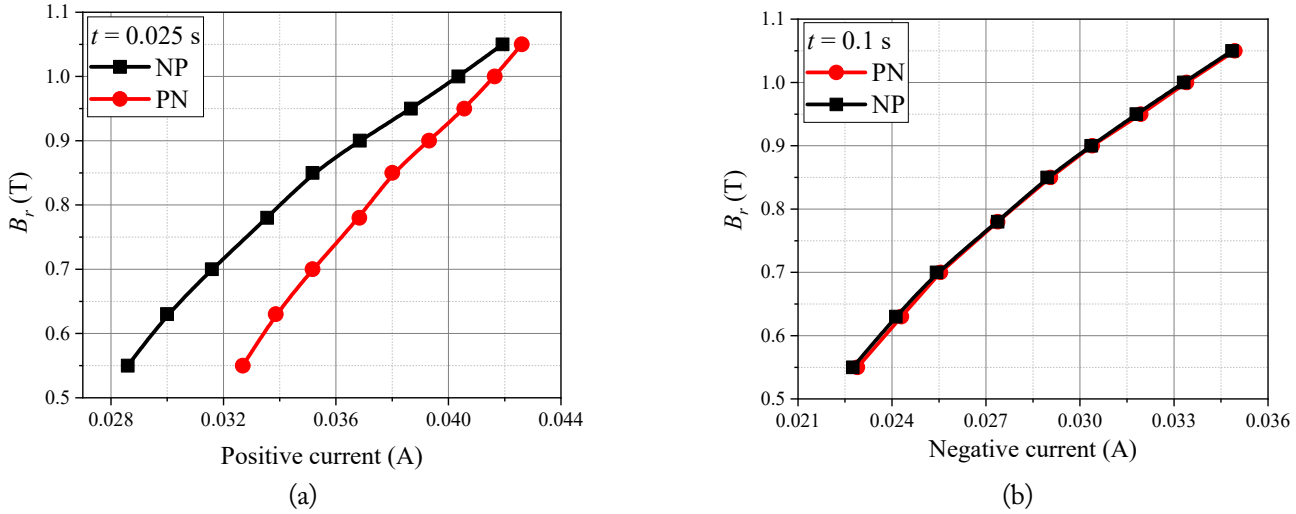

Fig. 10. (a) Relationship between positive respond current and B_r at t = 0.025 seconds and (b) relationship between negative respond current and B_r at t = 0.1 seconds.

built to verify the feasibility of the theoretical analysis and the accuracy of the proposed method. Fig. 11 shows a photograph of the experimental platform, where the tested core ("1") is composed of Baosteel B30P105 silicon steel sheets. The material type was kept consistent with the simulation to ensure the accuracy of the test results. Furthermore, a signal generator ("2") is employed to generate different square wave voltage signals, which can help realize the control of voltage polarity. A power amplifier ("3") is used to amplify the applied voltage signal, while a switch ("4") is employed to control the turn-on and turn-off actions of the detection circuit. The resistor ("5") is used to block the current. An oscilloscope ("6") is added to observe the flow of the current through the windings ("7"). Furthermore, the high-precision current probe N2782B ("8") is used to acquire current signals since it can realize accurate current detection in the ms or even the μs range. Moreover, Fluxmeter480 ("9") is included in the setup, since it is capable of tracking real-time changes in magnetic flux density, with the measured magnetic flux being the flux based on the voltage integration principle.

The initial RF direction of offline transformers usually remains unknown. At this moment, the same positive voltage as the initial RF polarity can be applied to measure the positive response current $i_+(t)$. Subsequently, when applying negative voltage, the negative current $i_-(t)$ can be measured. Subsequently, if the change rate of the $i_+(t)$ is found to be greater than $i_-(t)$, $i_+(t)$ can be determined to be $i_p(t)$, and $i_-(t)$ as $i_n(t)$, which would prove that the iron core has positive RF. If the opposite result is achieved, the iron core can be presumed to have negative RF. Finally, when $t = t_s$, the value of the negative current can be integrated using Eq. (13) to calculate the RF in the iron core.

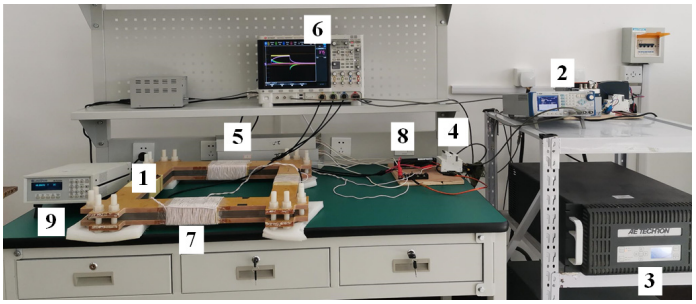

Fig. 11. The experimental platform.

Fig. 12 shows the voltage and respond current waveforms when the preset B_r is 0.846 T. This shows that when the positive voltage is loaded, $i_p(t)$ is generated, whereas when the negative voltage is loaded, $i_n(t)$ is generated. Fig. 13 shows the $i_p(t)$ and $i_n(t)$ at different RFs. It is evident that the change rate of $i_p(t)$ is faster than that of $i_n(t)$, as a result of which the iron core is determined to have a positive RF. This conclusion also indicates that $i_p(t)$ represents the positive RF direction and $i_n(t)$ represents the negative RF direction. Furthermore, the above analysis proves the accuracy of the theoretical analysis conducted in this paper.

As shown in Fig. 13, when the time is 0.1 seconds, the voltage is removed. At this time, the negative current was measured to calculate the RF in the iron core. Therefore, when $t_s = 0.1$ seconds, the negative current was measured and then substituted into Eq. (13) to calculate the RF in the iron core, represented as B_{r1}. In the case of PN, as shown in Fig. 13(a), when the preset RF is 0.922 T, the current value reaches 0.0311 A, with the calculated B_{r1} value being 0.929 T. Compared to the preset B_r, the relative error was found to be 0.76%. Meanwhile, in the case of NP, as shown in Fig. 13(b), when the preset B_r is 0.935 T, the calculated B_{r1} value reaches 0.946 T, with the relative error being 1.18%. This indicates that the change rate of RF is greater for NP than for PN. As a result, this paper primarily analyzed the measurement error in the case of NP.

Based on [6–8], RF is usually approximated as 0.2–0.7 times the saturation magnetic density. Since the saturated magnetic density of the iron core material selected for study in this paper was about 1.8 T, the RF detection range was determined to be 0.4 T to 1.2 T. Table 1 shows the experiment results at NP, with B_{r2} indicating the measured RF obtained using the voltage integration method [15, 16]. The relative error between the pre-

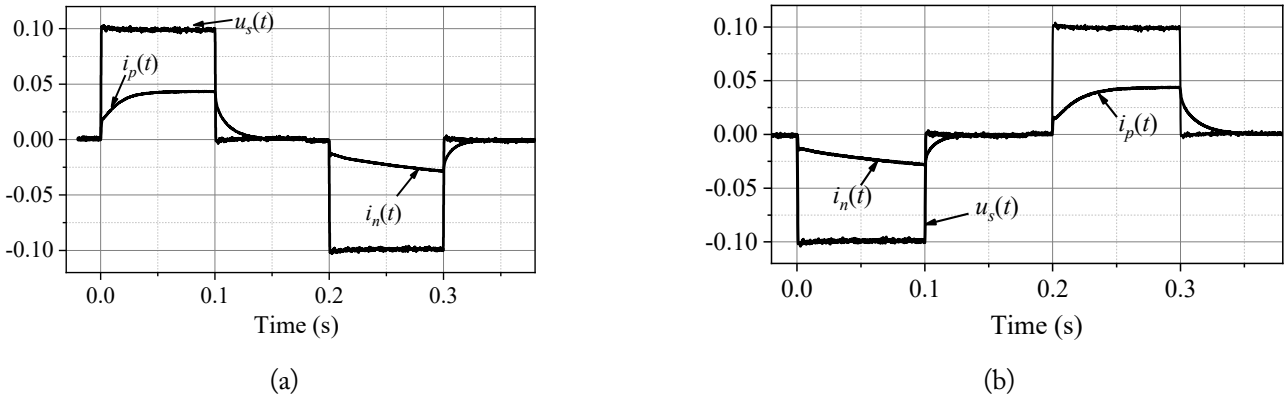

Fig. 12. Waveforms of applied DC voltage and measured current when B_r is 0.846 T: (a) PN and (b) NP.

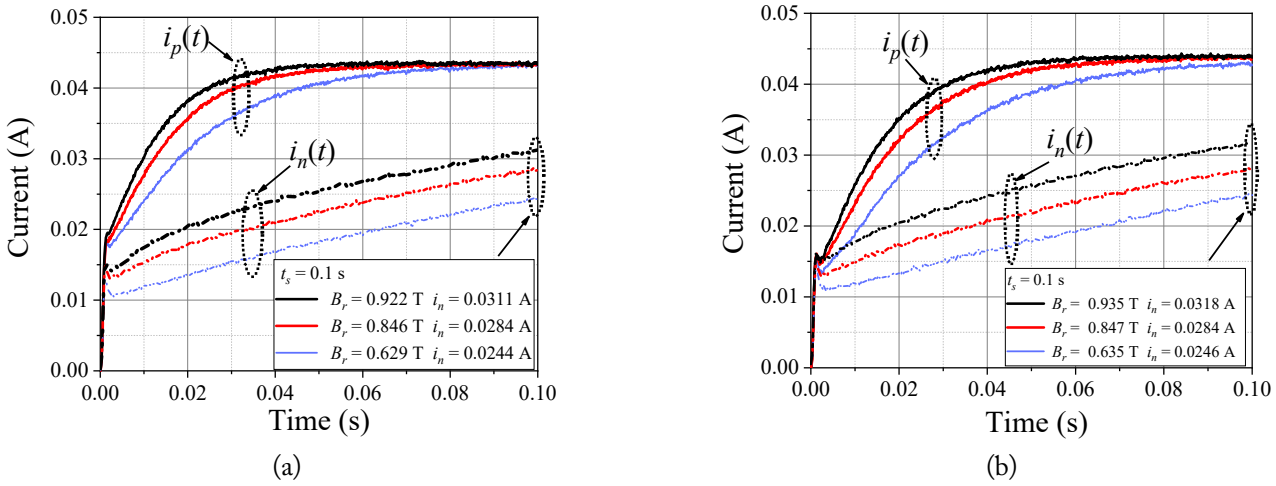

Fig. 13. Waveforms of measured currents at different residual fluxes: (a) PN and (b) NP.

Table 1. Experiment results at NP

Preset RF (T)	i_n (A)	B_{r1} (T)	B_{r2} (T)	ε_1% (%)	ε_2% (%)
0.548	0.0229	0.569	0.494	3.87	−9.81
0.635	0.0243	0.646	0.575	1.67	−9.40
0.678	0.0251	0.686	0.619	1.14	−8.77
0.800	0.0272	0.781	0.729	−2.37	−8.88
0.847	0.0285	0.834	0.776	−1.55	−8.42
0.895	0.0298	0.883	0.821	−1.36	−8.24
0.935	0.0316	0.946	0.857	1.12	−8.35
0.961	0.0324	0.970	0.877	0.95	−8.71

set RF and B_{r1} is expressed as ε_1%, while the relative error between the preset RF and B_{r2} is expressed as ε_2%. The maximum ε_1% is within 5%, which is less than the ε_2% obtained using a different preset B_r. This result highlights that the accuracy of the proposed method is higher than that of the voltage integration method.

Fig. 14 presents a comparative analysis of the simulation and experimental results at different RFs. It is observed that the variation trend of the experimental results is largely the same as that of the simulation results. Furthermore, the measurement error indicated that the proposed detection method exhibits a certain feasibility. Compared to existing detection methods [15–20], the proposed method was able to not only judge the RF direction, but also accurately detect the RF value. In addition, since the RF generation mechanism is closely related to variations in the differential permeability at the RF, the differential permeability may be significantly reflected by the measured response current. Furthermore, the proposed method can be applied for RF detection in other power equipment composed of iron cores, indicating its wide applicability.

V. Conclusion

In this paper, an indirect RF detection method for power transformer cores is proposed based on the different polarities of

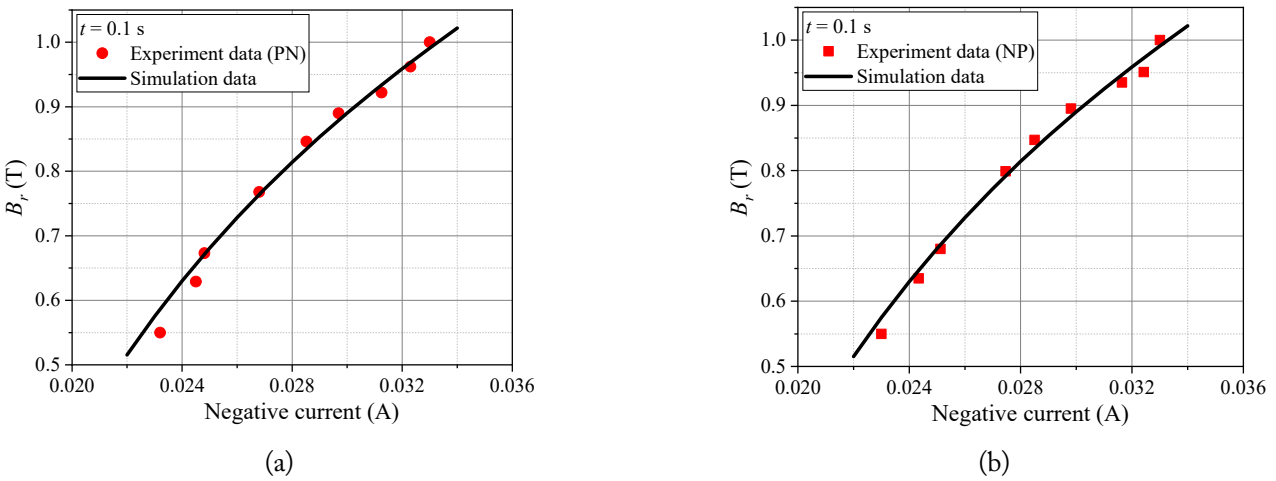

Fig. 14. Comparison of error results: (a) PN and (b) NP.

respond currents. The proposed method was able to accurately identify RF polarity and conduct a quantitative detection of the RF value. In particular, RF polarity was determined by comparing the change rates of different polarities of response currents. Furthermore, the relationship between the RF and the negative response current was constructed using the field-circuit coupling method to realize the quantitative detection of the RF value. The experimental results exhibited an accuracy that reached 5%, which is higher than the accuracy achieved by the existing methods. Notably, since transformer cores composed of different structures use different empirical formulas for RF calculation, their corresponding empirical formulas need to be extracted based on the presented method. The method proposed in this paper can also be applied to detect RF in other power equipment cores characterized by closed magnetic circuit structures.

This work was supported in part by the Science and Technology Program of Changzhou, China (No. CJ20235049), in part by the National Science Foundation of the Jiangsu Higher Education Institutions of China (No. 23KJB470009), in part by the Jiangsu Province Industry University Research Cooperation Project (No. FZ20230272), and in part by the Changzhou Science and Technology Support Project (No. CE20235045).

REFERENCES

[1] Q. Liu, F. Liu, R. Zou, S. Wang, Y. Tian, Y. Wang, L. Yuan, and Y. Li, "A compact-design oriented shipboard power supply system with transformer integrated filtering method," *IEEE Transactions on Power Electronics*, vol. 37, no. 2, pp. 2089-2099, 2022. https://doi.org/10.1109/TPEL.2021.3102938

[2] G. Glazyrin, N. Mitrofanov, A. Rusina, V. Fyodorova, and A. Arestova, "Simulation of transients in an autonomous power system considering the generator and transformer magnetic core saturation," *Energy Reports*, vol. 9(Supplement 1), pp. 444-451, 2023. https://doi.org/10.1016/j.egyr.2022.11.031

[3] S. Sanati and Y. Alinejad-Beromi, "Fast and complete mitigation of residual flux in current transformers suitable for autoreclosing schemes using Jiles-Atherton modeling," *IEEE Transactions on Power Delivery*, vol. 37, no. 2, pp. 765-774, 2022. https://doi.org/10.1109/TPWRD.2021.3070075

[4] S. Afrasiabi, M. Afrasiabi, B. Parang, M. Mohammadi, H. Samet, and T. Dragicevic, "Fast GRNN-based method for distinguishing inrush currents in power transformers," *IEEE Transactions on Industrial Electronics*, vol. 69, no. 8, pp. 8501-8512, 2022. https://doi.org/10.1109/TIE.2021.3109535

[5] E. Hajipour, M. Salehizadeh, M. Vakilian, and M. Sanaye-Pasand, "Residual flux mitigation of protective current transformers used in an autoreclosing scheme," *IEEE Transactions on Power Delivery*, vol. 31, no. 4, pp. 1636-1644, 2016. https://doi.org/10.1109/TPWRD.2015.2480773

[6] E. Colombo and G. Santagostino, "Results of the inquiries on actual network conditions when switching magnetizing and small inductive currents and on transformer and shunt reactor saturation characteristics," *Electra*, vol. 94, pp. 35-53, 1984.

[7] J. H. Brunke and K. J. Frohlich, "Elimination of transformer inrush currents by controlled switching. I. Theoretical considerations," *IEEE Transactions on Power Delivery*, vol. 16, no. 2, pp. 276-280, 2021. https://doi.org/10.1109/61.915495

[8] Y. F. Wu, H. R. Hu, W. Luo, T. Wang, and L. Ruan, "Research on no-load test of 1,000kV ultra-high voltage transformer," in *Proceedings of the 2011 Asia-Pacific Power and Energy Engineering Conference*, Wuhan, China, 2011, pp. 1-6. https://doi.org/10.1109/APPEEC.2011.5747683

[9] K. Wang, G. Li, S. Zhang, J. Li, J. Liu, X. Wu, H. Yang, and X. Hu, "Research on residual flux characteristics of transformer with single-phase four-limb core under different DC excitation current," in *Proceedings of 2020 IEEE International Conference on High Voltage Engineering and Application (ICHVE)*, Beijing, China, 2020, pp. 1-5. https://doi.org/10.1109/ICHVE49031.2020.9279826

[10] Y. Li, M. Jin, H. Li, G. Li, W. Chen, D. Chen, and J. Xie, "Study on measurement method of remanence of power transformer," *Power System Protection and Control*, vol. 47, no. 15, pp. 102-107, 2019. https://doi.org/10.7667/PSPC20191514

[11] T. Liu, X. Liu, S. Liang, J. Wang, and C. Yao, "Residual flux measuring method on the core of ferromagnetic components based on alternating polarity DC voltage source," *Transactions of China Electrotechnical Society*, vol. 32, no. 13, pp. 137-144, 2017.

[12] M. L. Hodgdon, "Applications of a theory of ferromagnetic hysteresis," *IEEE Transactions on Magnetics*, vol. 24, no. 1, pp. 218-221, 1988. https://doi.org/10.1109/20.43893

[13] D. Cavallera, V. Oiring, J. L. Coulomb, O. Chadebec, B. Caillault, and F. Zgainski, "A new method to evaluate residual flux thanks to leakage flux, application to a transformer," *IEEE Transactions on Magnetics*, vol. 50, no. 2, pp. 1005-1008, 2014. https://doi.org/10.1109/TMAG.2013.2282175

[14] C. Wei, X. Li, M. Yang, Z. Ma, and H. Hou, "Novel remanence determination for power transformers based on magnetizing inductance measurements," *Energies*, vol. 12, no. 24, article no. 4616, 2019. https://doi.org/10.3390/en12244616

[15] T. Zheng and Y. Wang, "Fast and in situ remanent flux detection method for a protection current transformer based on the fluxgate theory," *AIP Advances*, vol. 11, no. 1, article no. 015034, 2021. https://doi.org/10.1063/9.0000140

[16] D. Vulin, K. Milicevic, I. Biondic, and G. Petrovic, "Determining the residual magnetic flux value of a single-phase transformer using a minor hysteresis loop," *IEEE Transactions on Power Delivery*, vol. 36, no. 4, pp. 2066-2074, 2021.

https://doi.org/10.1109/TPWRD.2020.3019407
[17] Y. Ren, Y. Wang, C. Liu, and S. Wu, "A novel method for measuring residual flux density of the single-phase transformer core based on phase difference," *AIP Advances*, vol. 13, no. 2, article no. 025332, 2023. https://doi.org/10.1063/9.0000375
[18] S. Wu, Y. Ren, Y. Wang, C. Huo, and C. Liu, "Residual flux measurement of power transformer based on transient current difference," *IEEE Transactions on Magnetics*, vol. 58, no. 2, article no. 8400405, 2022. https://doi.org/10.1109/TMAG.2021.3082699
[19] C. Huo, Y. Wang, S. Wu, and C. Liu, "Research on residual flux density measurement for single-phase transformer core based on energy changes," *IEEE Transactions on Instrumentation and Measurement*, vol. 70, article no. 6011909, 2021. https://doi.org/10.1109/TIM.2021.3117087
[20] C. Huo, Y. Wang, S. Wu, Y. Yang, and Z. Zhao, "Residual flux density measurement method for transformer core considering relative differential permeability," *EEE Transactions on Magnetics*, vol. 57, no. 2, article no 8400204, 2021. https://doi.org/10.1109/TMAG.2020.3003658
[21] Z. Zhao, Y. Wang, and C. Huo, "Modeling of transformer ring core and residual magnetism measurement," *Electrical Measurement and Instrumentation*, vol. 60, no. 7, pp. 116-121, 2023.

Cailing Huo
https://orcid.org/0000-0001-5480-2007

received her M.E. degree in electrical engineering from Shanghai University of Electric Power, Shanghai, China, in 2015, and her Ph.D. degree in electrical engineering from Hebei University of Technology, Tianjin, China, in 2022. She is currently a lecturer at Jiangsu University of Technology, Jiangsu, China. Her research interests include the testing and elimination of remanence in transformer cores.

Fuyin Ni
https://orcid.org/0000-0003-4208-7928

received his Ph.D. degree in control engineering from Jiangsu University, Jiangsu, China. He is currently a vice professor at Jiangsu University of Technology, China. His research interests include modern power supply technology and distribution generation.

Yiming Yang
https://orcid.org/0000-0003-3181-5061

received his M.E. degree in electrical engineering from Hebei University of Technology, Tianjin, China, in 2021. He is currently a lecturer at Jiangsu University of Technology, Jiangsu, China. His research interests include magnetic materials and the measurement of soft magnetic composites.

Qiang Xie
https://orcid.org/0009-0005-2337-4456

received his M.E. degree in electrical engineering from the China University of Mining and Technology, Xuzhou, China, in 2014 and 2017. He is currently an engineer at the Changzhou Power Supply Branch of State Grid Jiangsu Electric Power Co. Ltd., where he is primarily engaged in the operation and overhaul of high-voltage cables.